Soller slit design and characteristics

Brian Bewer

Canadian Light Source, 101 Perimeter Road, Saskatoon, Saskatchewan, Canada S7N 0X4.
E-mail: brian.bewer@lightsource.ca

For X-ray absorption spectroscopy, either in transmission mode with concentrated samples or for dilute samples in fluorescence mode, it is advantageous to improve the signal-to-noise ratio by implementing a slit apparatus. Several investigations into the improvement of measurements when slits and filters are employed have been reported; however, these have always been for a particular design and are not transferable between dissimilar systems. A generalized approach to Soller slit design will be presented which enables a target level of noise rejection to be achieved by varying the number, size and placement of the filter and Soller slit assembly. A procedure for determining the reduction in efficiency of the Soller slits with respect to misalignment with the sample will also be discussed.

Keywords: Soller slits; Stern–Heald slits; Lytle detector; X-ray absorption spectroscopy.

1. Introduction

The benefits of removing signal noise from X-ray experiments have been well established in both radiology with anti-scatter grids (Hendee & Ritenour, 2002; Dendy & Heaton, 2003) and in spectroscopy with Soller slits (Soller, 1924; Stern & Heald, 1980; Tse *et al.*, 2011). In fluorescence X-ray absorption spectroscopy (XAS), with non-energy-dispersive detectors, the use of fluorescence-suppressing and scatter-removing slits combined with X-ray filters preferentially eliminates unwanted signal noise (Lytle *et al.*, 1975). With energy-dispersive detectors the combination of filters and slits reduces detector dead-time and non-linearities associated with concentrated samples (Cramer *et al.*, 1988).

Soller slits are designed with repeating blades constructed from a material which will absorb all or most of the X-rays that enter it and do not fluoresce in the energy range of interest. The distribution of scattered radiation from a synchrotron X-ray beam incident on a sample is calculable from the polarized variant of the Klein–Nishia equation,

$$\frac{d\sigma_{KN}}{d\Omega} = r_e^2 \kappa^2 \frac{\left\{1 + \frac{\gamma^2(1-\cos\theta)^2}{(1+\cos^2\theta)[1+\gamma(1-\cos\theta)]}\right\}}{[1+\gamma(1-\cos\theta)]^2},$$

$$\kappa^2 = \begin{cases} 1, & \sigma \text{ polarized,} \\ \cos^2\theta, & \pi \text{ polarized,} \end{cases}$$

(1)

where r_e is the classical electron radius, γ is the incident photon energy divided by the rest mass of the electron, and θ is the scattering angle measured from the direction of the incident photon (Jackson, 1999). For transmission XAS where there is a sample between ion chamber detectors commonly called I_0 and I_1 and a reference foil downstream between ion

chamber detectors I_1 and I_2, back scatter and contaminating fluorescence from the reference foil will enter I_1. Both of these contaminant signals can be substantially reduced by using Soller slits. This could either be a set of straight slits when using a line beam, or slits with blades having a varying pitch to focus on one spot for a pencil beam. In the case of fluorescence XAS, equation (1) indicates that the most suitable position for detector placement is orthogonal to the direction of the incident X-rays where there is a minimum in scattering cross-section amplitude. To preferentially eliminate scattered radiation from the sample a Soller slit and filter combination can be used. Each Soller slit blade is pitched to focus on the virtual source where the beam intersects the sample. In the following discussion, vertically gapped slits with horizontally parallel blades are examined in combination with a filter (Fig. 1), which can be used with a point source or a horizontal line source. This approach may be reconfigured for horizontally gapped slits with vertically parallel blades, or repeated for both orientations when a crossed-blade pattern in a grid formation is desired.

2. Discussion

The angular size of the Soller slit opening in Fig. 1 is $\theta_F = 2\arctan[(DS/2)/F]$. If there is a slit at each edge of the detection area and the slits are equally spaced in angle to cover equivalent regions of solid angle across the detector, the angular step between slits is $\Delta\theta = \theta_F/(N-1)$. The position in angle of the nth slit is $\theta_n = n\Delta\theta + \theta_0$, where θ_0 is an arbitrary angle that defines the starting orientation of the Soller slit apparatus and is the angle of the slit on the first edge of the detector. These angles for the N slits define spatial separations in the Soller slit holder between the blades, and position of
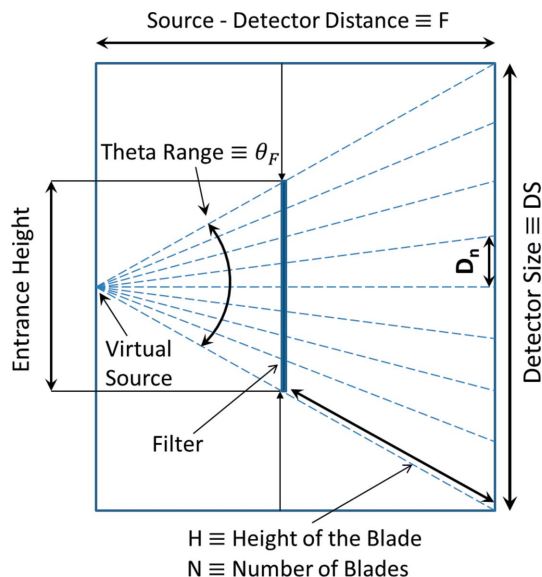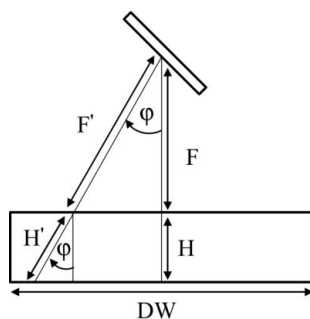
Figure 1
General outline of the Soller slit geometry and parameters.

the back of the blade in the linear holder is given by $D_n = \tan(\theta_n)F$ (Fig. 1). For focal distances where $F \simeq H$ there will be considerable distance changes between subsequent blade positions. For longer focus distances where $F \gg H$ there will be negligible distance changes between subsequent blade positions. In Fig. 1 only the height of the area detector is shown along the center line. This is because the ratios between the important geometric quantities will remain invariant for X-rays traveling along the width of the area detector allowing the value calculated for the center line of the detector to be used as an approximation over an arbitrarily sized detector. Fig. 2 shows how the ratio between the sample-to-detector distance (F) and the blade path length (H) will remain constant for X-rays traveling out of the central plane of the detector,

$$H'/F' = \frac{H/\cos\varphi}{F/\cos\varphi} = H/F. \quad (2)$$

Similarly the ratio between the blade path length (H) and the distance between blades (D), assuming they are positioned in a linear rack for equal solid angle spaces between them, will

Figure 2
For horizontally stacked blades the X-rays that travel along the width axis of the detector (DW) will have the ratio of the travel distance (F) and blade path length (H) remain constant for any angle φ.

Table 1
Owing to the thickness of the Soller slit blades, some of the fluorescence signal from the sample will be removed; using equation (3) the approximate value of the signal that passes through vertically spaced slits covering the full horizontal length of the detector is tabulated below for a 45.5 mm vertical detector size with 89 mm width, a 75 mm path from the virtual source to the detector, a 50 mm distance between the slit surface and the virtual source, and blade thickness of 0.15 mm.

Number of blades	Fraction of the sample fluorescence in the direction of the detector transmitted through the slits	Intrinsic efficiency of the slits with the chosen detector geometry
8	0.969	0.0481
9	0.964	0.0479
10	0.959	0.0476
11	0.954	0.0474
12	0.949	0.0471
13	0.943	0.0469

also be preserved. For fluorescence originating from the filter in front of the slits, the path difference from the sample is not relevant as the local geometry is the determining factor.

The length, width and thickness of the blades that cover the detector area determine the amount of signal from the sample that will be attenuated by the sum of all the blade surfaces. For this reason it is beneficial to use fewer blades with a larger height rather than more blades of small height whenever practical. The intrinsic efficiency is defined as the fraction of the signal from the sample that is not absorbed by the finite thickness of the slit material. This value can be easily found for spherically shaped Soller slits since the distance from the virtual source to any position on the blades vertically and horizontally across the detector area is constant. For the more common box-shaped Soller slits with straight vertically stacked slits having linear horizontal blades, the intrinsic efficiency of the spherical case is used as an approximation and will be a close approximation for $F \gg DS$,

$$\mathrm{Eff}^{\mathrm{Int}} \simeq \frac{\left[\theta_F - (N-2)\arctan\left(\frac{\mathrm{Blade\ width}/2}{F-H}\right)2\right]}{\theta_F} \frac{\theta_F\,\theta_W}{4\pi}, \quad (3)$$

where $\theta_F = 2\arctan[(DS/2)/F]$ and $\theta_W = 2\arctan[(DW/2)/F]$ are the angular height and width of the detector at a distance F away from the sample; it is assumed that the two slits on the upper and lower edge of the detector are just outside the field of view and thus block no signal from the sample, and $\arctan[(\mathrm{Blade\ width}/2)/(F-H)]$ is one half of the angular size of a centered blade defined by a right triangle where the virtual source, the center of the blade and one edge of the blade are the points of the right triangle. The intrinsic efficiency can be increased by using progressively thinner blades; however, reducing the blade thickness will decrease the total absorption length of the slits and thus reduce the fraction of X-rays that are stopped by the blades. Also, if the blades are made too thin they will not be firm enough to support their own weight. Table 1 lists intrinsic efficiency fractions for a Soller slit design with varying numbers of blades, each with 0.15 mm thickness. In the case where $F \simeq DS$, the angular size of each blade or pair of blades must be considered separately

Table 2
The fractions of isotropically emitted fluorescence originating at a filter attached to the front of the Soller slits that will pass through vertically spaced slits covering the full horizontal length of the detector are tabulated for varying blade heights, $2\arctan[(D/2)(1/H)]/\pi$; the vertical size of the detector used is 45.5 mm, the thickness of the blades is 0.15 mm, and the distance from the sample to the detector is assumed to be greater than the detector size so that $D_n \cong D_{n-1}$.

Height of Soller slit blade (mm)	Number of Soller slit blades					
	8	9	10	11	12	13
10	0.200	0.176	0.158	0.142	0.130	0.119
15	0.136	0.119	0.106	0.096	0.087	0.080
20	0.103	0.090	0.080	0.072	0.066	0.060
25	0.082	0.072	0.064	0.058	0.053	0.048

and summed to determine the total angular area that is obstructed. Thus, for $F \simeq DS$ the intrinsic efficiency is given by

$$\mathrm{Eff}^{\mathrm{Int}} \cong \frac{\left[\theta_F - \sum_2^{n-1} \arctan\left(\frac{\mathrm{Blade\ width}/2}{F_n - H}\right) 2\right]}{\theta_F} \frac{\theta_F \theta_W}{4\pi}, \qquad (4)$$

where it is again assumed that the two outermost blades are just outside the detection area.

For transmission XAS where the Soller slits are against the reference foil, or fluorescence XAS using a filter and Soller slits, the fraction of isotropically emitted fluorescence originating from the filter or foil surface facing the detector which does not pass through the slits is closely approximated by $2\arctan[(D/2)/H]/\pi$ for linearly stacked Soller slits (Fig. 3a). The angle range from the filter or foil surface in the direction of the detector that X-rays may freely pass through linearly stacked Soller slits is approximately given by $2\arctan[(D/2)/H]$ [Fig. 3(b), Table 2]. The first point in
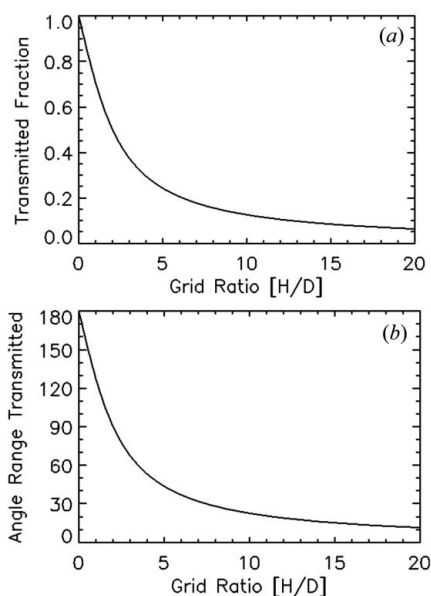
Fig. 3(b) corresponds to a slit with no height and allows any X-rays originating from the surface of the filter in a 180° arc to travel to the detector. As the height of the slits becomes larger and spacing between slits becomes smaller, the allowed path to the detector is reduced and thus the range of angles becomes smaller.

3. Results

To determine the total efficiency of the Soller slits it is necessary to know not only the intrinsic efficiency and the attenuated fraction of radiation but also the sensitivity of the Soller slits to misalignments of the sample and hence virtual source position. Using the derivation in Appendix A1 for the geometry in Fig. 5 the fraction transmitted through the Soller slits when the sample is closer than the intended focus is shown in Fig. 4(a) for varying number of blades. Similarly Fig. 4(b) plots the fraction transmitted through the Soller slits when the sample is further away than the intended focus for varying number of blades using the derivation in Appendix A2 and the geometry from Fig. 6. In Appendix A3 the calculation of efficiency changes owing to a lateral misalignment of the sample not in the direction of the stacked blades is discussed and the results can be expressed in terms of the vertical misalignments already examined (Fig. 7). In all cases the total efficiency of the Soller slits is the product of the intrinsic efficiency of the blades (Table 1) multiplied by the sum of the utilized portion of each blade gap [Figs. 4(a) and 4(b)],

$$\mathrm{Eff}^T = \mathrm{Eff}^{\mathrm{Int}} \frac{\sum_1^{n-1} \mathrm{Eff}_n^\theta}{N - 1}. \qquad (5)$$

In conclusion, the efficacy of Soller slit arrangements can be determined for spectroscopy systems. Desired reductions of

Figure 3
The fraction of isotropically emitted fluorescence from the filter passing through the grid is shown in (a). The range of angles measured from the surface of the filter in the direction of the detector allowed through the grid is shown in (b). Both are plotted as a function of grid ratio (H/D).
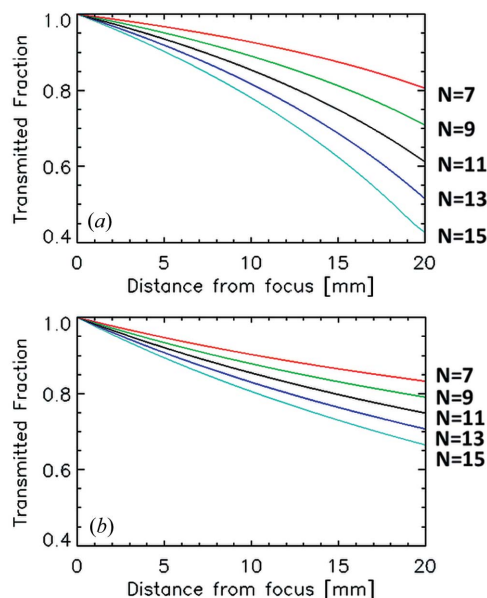

Figure 4
For a 45.5 mm tall detector face, a Soller slit focus point 50 mm away and 25 mm tall slit blades the reduction in slit efficiency, $\left(\sum_1^{n-1} \mathrm{Eff}_n^\theta\right)/(N-1)$, is plotted (a) when the sample is closer than the focus distance and (b) when the sample is further away than the focus distance.

signal noise can be achieved by changing the blade height, the number of blades and the focus distance for a given detector arrangement and blade orientation. The sensitivity of the resulting apparatus to misalignments can also be determined and it was shown that misalignments that bring the sample closer than the focus or move the sample laterally from the focus are more detrimental than the sample moving further away than the intended Soller slit focus for pitched blades. In the case of a virtual line source that is parallel to the blades the analysis will also provide an accurate efficiency estimate provided the length of the virtual line source is significantly smaller than the length of the blades and appropriately centered. In the case of a virtual point source where a grid pattern with both horizontal and vertical slits are desired, the efficiency can be determined by taking the product of the individually determined horizontal and vertical cases. This result will slightly underestimate the true performance of the grid pattern because the points where the horizontal and vertical slits cross each other will be counted twice, once in each of the intrinsic efficiency calculations for the two orientations.

For Lytle style detectors there is a virtual line source that is at a 45° angle to the filter, slits and detector. Owing to the sample geometry the distance of the virtual source from the slits changes across the line. The presented approach may still be used for Lytle detectors provided the slit apparatus was made to have a uniform sample solid angle between each pair of slits along their whole length. In this case the path length over the blades varies appropriately with the changing X-ray angle and thus the distance of the virtual source for any point on the 45° line maintains a constant level of filter-related fluorescence rejection (as discussed in Fig. 2). These conditions can be summarized as the gap between the blades (D) and the height of the blades (H) remain at a constant ratio D/H for a constant sample solid angle. For such a case the efficiency of the Lytle detector assembly can be determined from averaging a subset of point efficiencies along the line containing the sample.

APPENDIX A
Soller slit efficiency with an out-of-position sample

The derivations for Soller slit efficiencies owing to the sample being out of position will be presented for three cases: where the sample is (i) laterally in line and closer than the focus distance; (ii) laterally in line and further away than the focus distance; and (iii) laterally out of position at the focus distance along the axis of the blade. In each case it is given that

$$
\begin{aligned}
\theta_F &= \arctan[(DS/2)/F], \\
\Delta\theta &= \theta_F/(N-1), \\
\theta_n &= n\Delta\theta + \theta_0, \\
D_n &= \tan(\theta_n)F, \\
F_n &= F - H/\cos(n\Delta\theta).
\end{aligned} \tag{6}
$$

A1. Sample too close to the slits

Fig. 5 shows one side of the Soller slit apparatus and the geometric convention used to find the portion of the gap between blades that has a line of sight to the sample. What is found for the nth blade in this geometry also holds for the $-n$th blade on the opposite side of the geometric center as the sample is assumed to be centered laterally,

$$
\begin{aligned}
h_n &= \left[(D_n - D_{n-1})^2 + H^2 - 2(D_n - D_{n-1})H\cos(90 + n\Delta\theta)\right]^{1/2} \\
&= \left[(D_n - D_{n-1})^2 + H^2 + 2(D_n - D_{n-1})H\sin(n\Delta\theta)\right]^{1/2}, \tag{7}
\end{aligned}
$$

$$
\frac{\sin(\psi_n)}{H} = \frac{\sin(90 + n\Delta\theta)}{h_n} \Rightarrow \psi_n = \arcsin\left[\frac{H\cos(n\Delta\theta)}{h_n}\right], \tag{8}
$$

$$
y_n = \tan(\psi_n)\,D_n, \tag{9}
$$

$$
y' = F - y_n, \tag{10}
$$

$$
v_n^2 = y'^2 + F_n^2 - 2y'F_n\cos\theta_{n-1}, \tag{11}
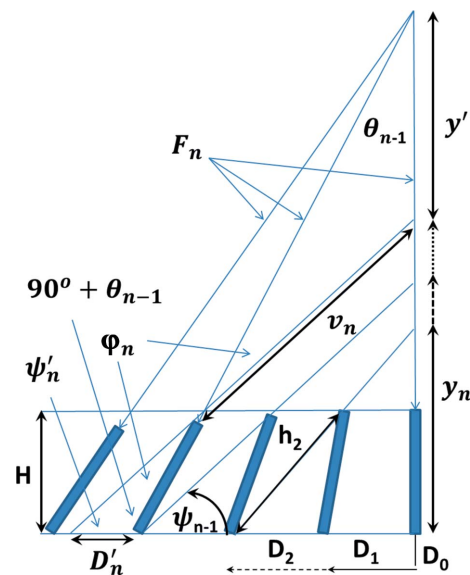$$

$$
y'/\sin\varphi_n = v_n/\sin\theta_{n-1}, \tag{12}
$$

$$
\varphi_n = \arcsin\left(\frac{y'_n}{v_n}\sin\theta_{n-1}\right), \tag{13}
$$

$$
\psi'_n = 180° - (90° + \theta_{n-1}) - \varphi_n = 90 - \theta_{n-1} - \varphi_n, \tag{14}
$$

$$
\frac{\sin\psi'_n}{H} = \frac{\sin\varphi_n}{D'_n}, \tag{15}
$$

$$
D'_n = \frac{\sin\varphi_n}{\sin\psi'_n}H, \tag{16}
$$

$$
\Delta\theta'_n = (1 - D'_n/D_n)\Delta\theta_n, \tag{17}
$$

Figure 5
Half of a Soller slit geometry is shown along with angle and length variable definitions for calculating the Soller slit efficiency when the sample is closer than the intended focus.

$$\text{Eff}_n^\theta = \Delta\theta_n'/\Delta\theta_n. \tag{18}$$

The total efficiency of the Soller slits is the intrinsic efficiency multiplied by the sum of all the gap efficiencies between the blades,

$$\text{Eff}^T = \text{Eff}^{\text{Int}} \frac{\sum_1^{n-1} \text{Eff}_n^\theta}{N-1}. \tag{19}$$

A2. Sample too far away from the slits

Fig. 6 shows one side of the Soller slit apparatus and the geometric convention used to find the portion of the gap between blades that has a line of sight to the sample. What is found for the nth blade in this geometry also holds for the $-n$th blade on the opposite side of geometric center as the sample is assumed to be centered laterally,

$$
\begin{aligned}
z_n^2 &= F_n^2 + y'^2 - 2F_n y' \cos(180° - \theta_n) \\
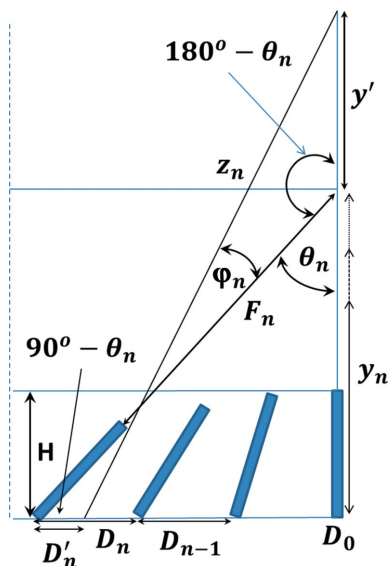&= F_n^2 + y'^2 + 2F_n y' \cos(\theta_n),
\end{aligned} \tag{20}
$$

$$\frac{\sin\varphi_n}{y'} = \frac{\sin(180° - \theta_n)}{z_n}, \tag{21}$$

$$\varphi_n = \arcsin\left(\frac{y'}{z_n}\sin\theta_n\right), \tag{22}$$

$$\frac{D_n'}{\sin\varphi_n} = \frac{H}{\sin\left[180 - (90 - \theta_n) - \varphi_n\right]}, \tag{23}$$

$$D_n' = H\frac{\sin\varphi_n}{\cos(\theta_n - \varphi_n)}, \tag{24}$$

$$\Delta\theta_n' = (1 - D_n'/D_n)\,\Delta\theta_n, \tag{25}$$

Figure 6
Half of a Soller slit geometry is shown along with angle and length variable definitions for calculating the Soller slit efficiency when the sample is further away than the intended focus.

$$\text{Eff}_n^\theta = \Delta\theta_n'/\Delta\theta_n. \tag{26}$$

The total efficiency of the Soller slits is the intrinsic efficiency multiplied by the sum of all the gap efficiencies between the blades,

$$\text{Eff}^T = \text{Eff}^{\text{Int}} \frac{\sum_1^{n-1} \text{Eff}_n^\theta}{N-1}. \tag{27}$$

A3. Lateral sample misalignment orthogonal to the blade direction

Fig. 7 shows one side of the Soller slit apparatus and the geometric convention used to find the portion of the gap between blades that has a line of sight to the sample. What is found for the nth blade in this geometry does not hold true for the $-n$th blade on the opposite side of geometric center. However, the nth blade in this approach is similar to efficiency corrections when the virtual source is further away than the focus. To find the $-n$th blade correction a similar approach to efficiency changes when the virtual source is closer than the focus should be used. In both cases the vertical separation between the slits and the sample is assumed to be the correct focus distance,
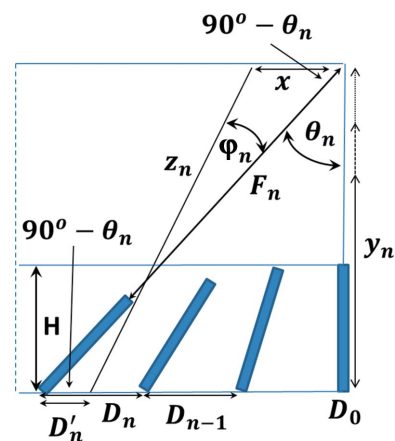
$$z_n = F_n^2 + x^2 - 2F_n x \cos(90 - \theta_n), \tag{28}$$

$$z_n = F_n^2 + x^2 - 2F_n x \sin(\theta_n), \tag{29}$$

$$\frac{x}{\sin\varphi_n} = \frac{z_n}{\sin(90 - \theta_n)}, \tag{30}$$

$$\varphi_n = \arcsin\left(\frac{x}{z_n}\cos\theta_n\right), \tag{31}$$

$$\frac{D_n'}{\sin\varphi_n} = \frac{H}{\sin\left[180 - (90 - \theta_n) - \varphi_n\right]}, \tag{32}$$

Figure 7
Half of a Soller slit geometry is shown along with angle and length variable definitions for calculating the Soller slit efficiency when the sample is laterally shifted away from the intended focus orthogonal to the length of the blades.

$$D'_n = H \frac{\sin \varphi_n}{\cos(\theta_n - \varphi_n)}, \tag{33}$$

$$\Delta\theta'_n = (1 - D'_n/D_n)\,\Delta\theta_n, \tag{34}$$

$$\mathrm{Eff}^\theta_n = \Delta\theta'_n/\Delta\theta_n. \tag{35}$$

The total efficiency of the Soller slits is the intrinsic efficiency multiplied by the sum of all the gap efficiencies between the blades,

$$\mathrm{Eff}^T = \mathrm{Eff}^{\mathrm{Int}} \frac{\sum_1^{n-1} \mathrm{Eff}^\theta_n}{N-1}. \tag{36}$$

References

Cramer, S. P., Tench, O., Yocum, M. & George, G. N. (1988). *Nucl. Instrum. Methods Phys. Res. A*, **266**, 586–591.

Dendy, P. P. & Heaton, B. (2003). *Physics for Diagnostic Radiology*, 2nd ed. Philadelphia: The Institute of Physics.

Hendee, W. R. & Ritenour, E. R. (2002). *Medical Imaging Physics*, 4th ed. New York: Wiley-Liss.

Jackson, J. D. (1999). *Classical Electrodynamics*, 3rd ed. New York: Wiley.

Lytle, F. W., Sayers, D. E. & Stern, E. A. (1975). *Phys. Rev. B*, **11**, 4825–4835.

Soller, W. (1924). *Phys. Rev.* **24**, 158–167.

Stern, E. A. & Heald, S. M. (1980). *Nucl. Instrum. Methods*, **172**, 397–399.

Tse, J. J., George, G. N. & Pickering, I. J. (2011). *J. Synchrotron Rad.* **18**, 527–529.